

# Effects of Four-Mode Hydrothermal Aging on Three-Way Catalysts for Passive Selective Catalytic Reduction to Control Emissions from Lean-Burn Gasoline Engine

C.R. Thomas, J.A. Pihl, M.J. Lance, T.J. Toops, J.E. Parks II and J. Lauterbach\*

## Abstract:

Passive selective catalytic reduction (SCR) is a promising approach for the control of  $\text{NO}_x$  emissions in lean burn gasoline exhausts. It requires ammonia ( $\text{NH}_3$ ) to be produced over a three-way catalyst (TWC) during periods of fuel-rich operation for the reduction of  $\text{NO}_x$  during periods of fuel-lean operation. Previous research has shown the viability of this system but has not examined the effects of hydrothermal degradation. This work is focused on evaluating the effects of hydrothermal aging on the TWC in a passive SCR system. Two catalysts were studied: a Pd-only TWC, and a  $\text{NO}_x$  storage TWC. Samples were aged at  $920^\circ\text{C}$  for 100 hours using a four-mode hydrothermal aging procedure. This causes the catalyst to be oxidized and reduced, as it would in a real system. The effects of aging were evaluated using simulated exhaust under both steady state and lean-rich cycling conditions. Hydrothermal aging caused significant changes in catalyst activity, leading to a decrease in low temperature conversion of carbon monoxide (CO) and propane ( $\text{C}_3\text{H}_8$ ) on both catalysts, and degradation of oxygen storage and  $\text{NO}_x$  storage components. However, the catalysts maintained their activity for  $\text{NO}_x$  conversion and  $\text{NH}_3$

---

\* This research was sponsored by the U.S. Department of Energy (DOE), Office of Energy Efficiency and Renewable Energy - Vehicle Technologies Office. This manuscript has been authored by UT-Battelle, LLC, under Contract No. DE-AC0500OR22725 with the U.S. Department of Energy. The United States Government retains and the publisher, by accepting the article for publication, acknowledges that the United States Government retains a non-exclusive, paid-up, irrevocable, world-wide license to publish or reproduce the published form of this manuscript, or allow others to do so, for the United States Government purposes. The Department of Energy will provide public access to these results of federally sponsored research in accordance with the DOE Public Access Plan (<http://energy.gov/downloads/doe-public-access-plan>).

production, showing sufficient activity for the operation of a passive SCR with an optimum projected fuel consumption of 92-98% compared to stoichiometric operation.

## **1. Introduction**

Despite the growing prevalence of alternative fuels and renewable energy, petroleum based fuels accounted for 92% of transportation energy use in 2016 [1]. Furthermore, 54% of that petroleum energy was consumed by gasoline engines in cars and light trucks. This significant portion of the United States energy consumption represents a viable opportunity for combatting the rising demand for petroleum in the United States. Even a modest increase in the fuel economy of these small gasoline engines can have a significant impact on the total United States petroleum consumption. However, any technology that is used to improve fuel efficiency in these engines must also comply with increasingly strict emissions regulations. EPA tier 3 regulations require both increased fuel efficiency and decreased emissions compared to previous regulations [2].

Lean burn engines are a promising technology to improve fuel economy. By combusting gasoline with a high air-fuel ratio (AFR), lean burn engines provide increased fuel efficiency and, by extension, decreased carbon dioxide (CO<sub>2</sub>) emissions. Research conducted by Parks *et al.* has shown that operating in a fuel lean environment can increase an engine's efficiency by up to 15% over stoichiometrically operated engines [3]. However, because conventional three-way catalysts are not able to reduce NO<sub>x</sub> emissions in this oxygen-rich exhaust, leading to NO<sub>x</sub> emissions up to 0.35 g/mile, far exceeding the 0.03 g/mile limit set by EPA Tier 3 regulations. These elevated NO<sub>x</sub> emissions are a significant hurdle and currently the primary obstacle to the widespread commercial implementation of lean burn engines.

The primary methods for the elimination of NO<sub>x</sub> in oxygen-rich exhausts fall into two categories: NO<sub>x</sub> storage and reduction (NSR) and selective catalytic reduction (SCR) [4]. The first

NSR systems were designed by Toyota in the mid 1990's [5]. Since then, NSR systems have seen some commercial success, being implemented by various automobile manufacturers over the last 20 years. Much like standard TWCs, NSR catalysts generally use platinum group metals (PGM) for the oxidation and reduction reactions. In addition, these NSR catalysts also incorporate barium as a NO<sub>x</sub> storage component. NO<sub>x</sub> in the exhaust can be stored on the barium as a nitrate species for later reduction [6]. To reduce the NO<sub>x</sub>, NSR systems require the engine to run with an excess of fuel for a brief period to provide reductants capable of reacting with the nitrates on the surface. While these systems have been used in several vehicles, NO<sub>x</sub> will often only be partially reduced to N<sub>2</sub>O, a very strong greenhouse gas, or it can desorb without reacting, preventing the system from meeting emission regulations [7,8].

Another approach to NO<sub>x</sub> control in lean exhausts is SCR using either hydrocarbons or urea as a reductant. Urea is the most commercially successful reductant, being implemented into both stationary pollution sources and heavy-duty diesel engines. In a urea-SCR system, the NO<sub>x</sub> reduction generally takes place on a separate, specialized catalyst, while the oxidation reactions take place upstream on a more typical three-way catalyst [9,10]. This is unlike the NSR system, where the oxidation of CO and hydrocarbons take place on the same catalyst as the NO<sub>x</sub> storage and reduction. The most common SCR catalysts are vanadia and ion-exchanged zeolites, containing either iron or copper [11–14]. In these systems, an aqueous solution of urea is injected into the hot exhaust after the oxidation catalyst. The urea is rapidly hydrolyzed to ammonia (NH<sub>3</sub>), which then reduces the NO<sub>x</sub> in the exhaust primarily through standard SCR and fast SCR reactions, shown in equations 1 and 2.



The full mechanism, surface species formed, and rate limiting step of urea-SCR on a Cu-zeolite catalyst were studied by Janssens *et al.* They concluded that these two reactions form a complementary reaction cycle, where the rate-limiting step is the oxidation of NO into a nitrate on the Cu site [15].

There are some concerns with implementing urea-SCR systems for lean burn gasoline engines. While they have proven effective in reducing NO<sub>x</sub> emissions in diesel exhaust systems, they require several additional design considerations over traditional, stoichiometrically operated gasoline systems. First, they require an additional tank to store the urea solution. This can be costly for a small vehicle where space is at a premium, and it can be off-putting to consumers to have an additional tank to fill. Second, they require a urea injection and control system. This can be expensive to produce for the automobile manufacturer since it requires several additional sensors and plumbing to transport and inject the urea [16,17]. A passive SCR system was proposed that would reduce NO<sub>x</sub> from lean burn engines without the need for a urea tank or an injection system [18]. This system requires periodic switching between a fuel rich phase, where NH<sub>3</sub> is produced over a close-coupled TWC, and a fuel lean phase where excess NO<sub>x</sub> can be reduced by NH<sub>3</sub> stored on a downstream SCR catalyst.

While a passive SCR system requires two catalysts, this research is focused on the close coupled TWC. TWCs have a long history of research and NH<sub>3</sub> has long been seen as a secondary pollutant from automobile exhaust. However, since it was recently proposed that it would be possible to use the NH<sub>3</sub> in the exhaust for SCR of NO<sub>x</sub>, research has been conducted on the promotion of NH<sub>3</sub> production on TWCs. The mechanism for NH<sub>3</sub> production was investigated by Rahkamaa-Tolonen *et al.* [19]. Their work indicated that NH<sub>3</sub> was produced through the adsorption of NO and H<sub>2</sub> on the PGM surface. H<sub>2</sub> rapidly dissociated into H species, while NO dissociation

is slower. Adsorbed H species can aid in the dissociation of NO, by reacting to form N and OH species on the surface. The adsorbed N and H species then reform into NH<sub>3</sub>. They reported that the dissociation of NO, which can be aided by adsorbed H species, is the rate limiting step for this reaction. Work by Oh and Triplett showed that the presence of CO in the exhaust stream can have beneficial effects on the reduction of NO<sub>x</sub> to NH<sub>3</sub> on Pd-based TWCs [20]. Their work showed that CO can benefit the system through the production of H<sub>2</sub> via the water gas shift reaction, aiding in the reduction of NO directly, and the formation of reactive intermediates, such as isocyanate species on the Pd surface. A study by Adams *et al.* focused on NH<sub>3</sub> production on platinum or palladium catalysts supported on Al<sub>2</sub>O<sub>3</sub> [21]. They found that both platinum and palladium on Al<sub>2</sub>O<sub>3</sub> were very effective for the production of NH<sub>3</sub>, however it was determined that palladium catalysts were more effective due to their activity for WGS and the potential for reactive intermediates to form on the surface, corroborating earlier evidence by Oh. Finally, previous studies within this research project have used simulated exhaust studies to show that TWCs can produce the required NH<sub>3</sub> during fuel rich operation to reduce NO<sub>x</sub> emissions, and still have up to 10% increased fuel economy []. These results were validated through engine testing, demonstrating the potential for passive SCR in a realistic system [22]. It is well documented that NH<sub>3</sub> production over TWCs is a viable route for the delivery of NH<sub>3</sub> to an SCR catalyst. However, the effect of hydrothermal aging on the long-term operation of a passive SCR system has not been thoroughly explored.

Hydrothermal aging of automotive catalysts has been a major concern since their inception. Investigations throughout the years has shown that metal sintering is one of the primary sources of catalyst deactivation during operation [23]. Researchers have looked at several methods to reduce metal sintering in TWCs, from promoters to the effects of different supports [24–26].

However, to date, there has not been an adequate method for maintaining small particles in realistic exhaust conditions. As such, an increase in metal particle size on the TWC will always occur during regular operation and continue throughout the useful life of a TWC. In some cases, this can lead to metal particle sizes over 40 nm [23]. Another consideration is the loss of interaction between the active metal and the oxygen storage component (OSC) present on the catalyst. The interaction between these species is beneficial for low temperature CO oxidation [27]. Beyond the sintering of the metal on these catalysts, the species responsible for oxygen storage (Ce) and NO<sub>x</sub> storage (Ba) can also deteriorate. Under aging conditions, ceria loses a large amount of surface sites from phase segregation and agglomeration on the surface [28]. NO<sub>x</sub> storage capacity (NSC) suffers from degradation through a different mechanism. While the barium does lose surface sites, the majority of its deactivation comes from the formation of barium aluminate and barium cerate at elevated temperatures [29]. The effects of hydrothermal aging on the SCR catalyst is also a concern. Previous work has shown that some Cu-zeolite SCR catalysts can degrade under hydrothermal conditions, particularly Cu-ZSM-5 [32]. However, as illustrated by Fickel et al. some small-pore Cu-zeolite formulations can show high hydrothermal resistance [33]. While the effects of SCR catalyst aging will be a concern for the real-world implementation of a passive-SCR system, the evaluation of these effects is outside of the scope of the current work.

Here, we examine the effects of 100 h of four-mode hydrothermal aging on two commercially formulated three-way catalysts for the purposes of implementation into a passive SCR system. This aging procedure exposes the catalyst to stoichiometric CO oxidation conditions in addition to periodic oxidizing and reducing conditions. These periodic oxidizing and reducing conditions are essential to model the aging of a catalyst in a passive-SCR system, where lean/rich cycling is a continuous process during operation. The metal particle size and CO light-off

temperature are monitored throughout the aging process. Furthermore, the activity of the fully aged catalyst samples is compared to the activity of degreened samples for both steady state and lean/rich cycling evaluations. The primary activities of concern in these evaluations are the conversion of CO, NO<sub>x</sub>, and hydrocarbons, as well as the production of NH<sub>3</sub>. Furthermore, in the lean/rich cycling experiments, changes in NO<sub>x</sub> storage and oxygen storage are also monitored.

## 2. Experimental

### 2.1 Catalyst Formulations

Catalyst samples are cut from commercially formulated catalyst monoliths in 2 cm diameter, 5 cm length cylindrical cores. Table 1 gives an overview of the catalysts being evaluated in this project. The Malibu-1 sample is taken from the front end of a dual zone TWC inside a 2009 Chevrolet Malibu. It contains palladium as the primary active metal on the surface, but also contains low loadings of other metals, including cerium and barium, as promoters. The ORNL-1 sample was provided by Umicore and contains platinum and rhodium, as well as cerium for oxygen storage, and barium for NO<sub>x</sub> storage. These catalysts were chosen for this work based on their high performance in previous reactor studies [30].

Table 1: Catalysts Studied

Catalyst ID	Description	Pt (g/L)	Pd (g/L)	Rh (g/L)	OSC	NSC
Malibu-1	Pd-Only TWC	0	7.3	0	Low	Low
ORNL-1	NSR Catalyst	2.47	4.17	0.05	High	High

### 2.2 Four-Mode Hydrothermal Aging Procedure and Apparatus

The apparatus used to conduct the catalyst aging uses four MKS Mass-Flo 1179A mass flow controllers to control the flow of 100% N<sub>2</sub>, CO<sub>2</sub>, CO, and O<sub>2</sub>. The water is introduced through a temperature controlled bubbler with N<sub>2</sub> flowing through it. The gases then flow through a Thermo

Scientific Lindberg/Blue M TF55035C tube furnace with a 2.5 cm quartz tube reactor. Two O<sub>2</sub> sensors (LCAN N6) are installed at the inlet and outlet of the reactor. These allow for monitoring of the oxygen content and ensure proper cycling. Inside of the reactor tube, quartz rods are used to help preheat the gas, and the catalyst is insulated just outside of the heated zone of the furnace, as shown in Figure 1. This allows for the catalyst to be heated through the exothermic CO oxidation, and more closely resembles a real system, where the catalyst itself is not heated. Omega K-type thermocouples are positioned at the inlet gas, catalyst inlet, catalyst mid bed, and catalyst outlet (Gas, In, Mid, Out, respectively). The mass flow rates, bubbler temperature, and furnace are all controlled through LabView on a connected PC, while the O<sub>2</sub> concentrations, and temperatures in the reactor tube are continuously recorded by the LabView program.

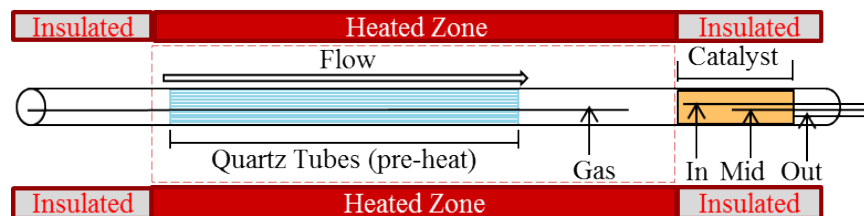


Figure 1: Hydrothermal aging reactor setup

During aging, the catalyst is first brought to aging temperature under stoichiometric operating conditions. Once it reaches the desired temperature, it begins cycling using the four-mode hydrothermal aging procedure shown in Table 2. It includes four phases in a six-minute cycle and a space velocity of 50,000 hr<sup>-1</sup>. The transition between the phases was controlled through the variation of O<sub>2</sub> and N<sub>2</sub> flow to maintain a constant space velocity. The first portion is a stoichiometric phase lasting for 330 s during which the catalyst is used for CO oxidation at 920°C in the presence of water. The second phase is a short fuel rich phase where the oxygen flow is

turned off, leading to reduction of the catalyst. Next, the catalyst is again operated under stoichiometric conditions for 10 seconds before transitioning to the fourth phase: a short fuel lean phase, where the O<sub>2</sub> flow is increased, while the N<sub>2</sub> and, by extension, the H<sub>2</sub>O are decreased to compensate. Catalyst samples were aged for 25, 50, and 100 hours using this procedure.

Table 2: Four mode hydrothermal aging procedure

	Time	H <sub>2</sub> O	CO <sub>2</sub>	CO	O <sub>2</sub>	N <sub>2</sub>
<b>Phase 1: Stoich</b>	330s	10%	10%	2%	1%	Bal.
<b>Phase 2: Rich</b>	10s	10%	10%	2%	0%	Bal.
<b>Phase 3: Stoich</b>	10s	10%	10%	2%	1%	Bal.
<b>Phase 4: Lean</b>	10s	9%	10%	2%	10%	Bal.

Each sample was aged in five segments, with the temperature being ramped down and back up between each segment. This means that the 25 hr aged sample was ramped up to 920°C under stoichiometric conditions, aged for 5 hours using the aging procedure, and then ramped back down under stoichiometric conditions. Similarly, the 50 hr aged sample was aged in 10 hr aging segments, and the 100 hr aged sample was aged in 20 hr segments. During the ramp up on each of these segments, the temperature in the catalyst mid bed ( $T_{Mid}$ ) increases sharply as the exothermic CO oxidation reaction lights off, as shown in Figure 2. By monitoring the point that  $T_{Mid}$  intersects with  $T_{Gas}$  it is possible to determine changes in the light-off temperature. While this number is not equivalent to the standard measurements of  $T_{90}$  or  $T_{50}$ , it does give an idea of the qualitative changes in CO oxidation light off during the hydrothermal aging process.

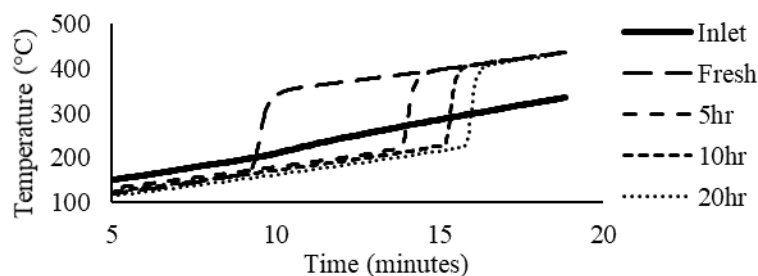


Figure 2: Light-off on Malibu-1 during first 20 hours of aging

After 25, 50 and 100 hours of aging, palladium particle sizes were determined using both STEM and H<sub>2</sub> chemisorption measurements. Samples for this evaluation were obtained by grinding the catalyst monolith. STEM images were taken on the TALOS system at the Oak Ridge National Laboratory's Low Activation Materials Development and Analysis (LAMDA) facility [31]. The particle sizes were determined by sampling at least 100 metal particles using high angle annular dark field (HAADF) images and energy dispersive x-ray spectroscopy (EDX) images. The chemisorption measurements were taken using H<sub>2</sub> titration on a Micromeretics AutoChem II Chemisorption Analyzer system, with a H<sub>2</sub> concentration of. The dispersion of Pd on the surface was determined, and particle size measurements were estimated assuming hemispherical metal particles.

### 2.3 Steady State Activity

The flow reactor used for steady state catalyst evaluation is equipped with MKS 1179A Mass-Flo controllers to control the flow of reactor gases including O<sub>2</sub>, CO, H<sub>2</sub>, NO, SO<sub>2</sub>, C<sub>3</sub>H<sub>8</sub>, CO<sub>2</sub>, and N<sub>2</sub>. Water is introduced to the system through a Eldex Optos HPLC pump. The catalyst is loaded into a 1-inch diameter quartz tube reactor, which is heated by a Thermo Scientific Lindberg/Blue M TF55035C tube furnace. From there, the gas is flowed into a MKS Multigas 2030 gas phase Fourier-Transform infrared (FTIR) spectrometer to measure the products.

Table 3: Gas compositions simulating various  $\lambda$  values

$\lambda$	0.95	0.96	0.97	0.98	0.99	1.00
O <sub>2</sub> (%)	0.96	1.02	1.07	1.13	1.17	1.22
CO (%)	2.0	1.8	1.6	1.4	1.2	1.0
H <sub>2</sub> (%)	1.0	0.9	0.8	0.7	0.6	0.5
NO (%)			0.06			
C <sub>3</sub> H <sub>8</sub> (%)			0.1			
H <sub>2</sub> O (%)			11			
CO <sub>2</sub> (%)			11			
SV (hr <sup>-1</sup> )			27,000			

Fresh and aged catalysts are evaluated in this reactor using a gas inlet temperature of 400 °C. The catalysts are tested under conditions simulating various AFRs as shown in Table 3. Here, AFR is measured using  $\lambda$ , which is the ratio of the used AFR to the stoichiometric AFR as shown in equation 3.

$$\lambda = \text{AFR}/\text{AFR}_{\text{stoich}} \quad (3)$$

This means that if  $\lambda$  is higher than 1, there is an excess of O<sub>2</sub> and the condition is lean. If it is lower than 1, there is an excess of reductants and the condition is rich. The reactor gas for these evaluations is composed of O<sub>2</sub>, CO, H<sub>2</sub>, NO, C<sub>3</sub>H<sub>8</sub>, H<sub>2</sub>O, CO<sub>2</sub>, and balanced with N<sub>2</sub> at a space velocity of 27,000 hr<sup>-1</sup>. Values of  $\lambda$  are varied through the flow of O<sub>2</sub>, CO, and H<sub>2</sub>. C<sub>3</sub>H<sub>8</sub> is chosen as the model hydrocarbon due to its difficulty in being oxidized under lean conditions, which allows us to evaluate this approach under a worst-case scenario basis [30]. During evaluations, the outlet steady state concentrations of four main components were analyzed: NH<sub>3</sub>, CO, C<sub>3</sub>H<sub>8</sub>, and NO<sub>x</sub>. From these concentrations, the conversion of NO, CO, and C<sub>3</sub>H<sub>8</sub> were calculated, as well as the production of NH<sub>3</sub>.

## 2.4 Cycling Activity

Cycling activity on the aged catalysts is measured in a flow reactor controlled through a LabVIEW program. The apparatus is equipped with MKS 1479A Mass-Flo controllers to control inlet gases. Water delivery is handled through an Eldex Optos HPLC pump. Switching between lean and rich operation is controlled through Valco medium temperature 1/8 inch switching valves. The catalyst is housed in a 25mm quartz tube heated by a Thermo Scientific Lindberg/Blue M TF55035C tube furnace. An omega K-type thermocouple is used to monitor the temperature of the gas entering the catalyst, and three more are used to monitor the catalyst temperature at the inlet, the middle, and the outlet. The contents of the gas leaving the reactor are monitored through gas phase FTIR and mass spectrometry. The FTIR used is an MKS Multigas 2030HS, while the mass spectrometer is a Pfeifer Vacuum PrismaPlus. During the experiments, the catalysts undergo constant cycling conditions as shown in Figure 3. A LabVIEW program integrates the outlet  $\text{NO}_x$  during the lean phase, switching to the rich conditions when the total  $\text{NO}_x$  reaches 0.027 mol/L catalyst. Then, the program monitors the outlet  $\text{NH}_3$ , and switches back to the lean conditions when the total  $\text{NH}_3$  reaches the same 0.027 mol/L catalyst. This threshold is 25% of the  $\text{NH}_3$  storage capacity on a Cu-zeolite catalyst of an equivalent volume.

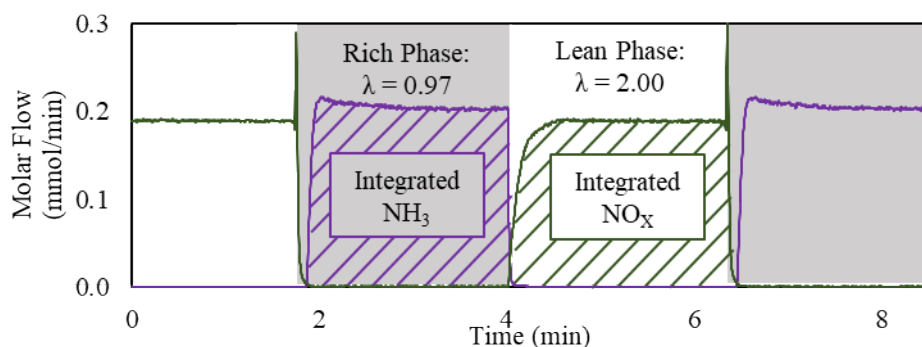


Figure 3: Time series data for  $\text{NO}_x$  and  $\text{NH}_3$  showing automated integration and switching method used for feedback-controlled cycling

Due to the lean/rich cycling, the temperature of the catalyst is changing constantly throughout the evaluation. Because of this, the results are reported as a function of the gas inlet temperature for all cycling experiments. The catalysts are tested under two separate cycling conditions, fixed load and load step. The fixed load condition simulates regular operation of the engine, where the same engine load is required for both the lean and rich phases. This means that the fuel being fed into the engine is constant, but during the lean phase, additional air is introduced to increase the  $\lambda$  value, leading to increased space velocity in the lean phase. Load step simulates the opportunistic production of  $\text{NH}_3$  during periods of high load on the engine. During these periods, the fuel introduced into the engine is increased, resulting in higher space velocity and increased temperatures in the engine. This period of increased load leads to high levels of  $\text{NO}_x$  being present in the engine exhaust, allowing for a large amount of  $\text{NH}_3$  to be produced and stored on the downstream SCR catalyst. These conditions are outlined in Table 4. Both conditions simulate cycling between a lean phase  $\lambda$  of 2.0 rich phase  $\lambda$  of 0.97, found to be the optimum in previous reactor and engine experiments. The aged catalysts are compared to catalysts degreened at  $700^\circ\text{C}$  for 16 hours in 10%  $\text{O}_2$ , 10%  $\text{H}_2\text{O}$ , balance  $\text{N}_2$ .

Table 4: Cycling experimental conditions

	Fixed Load		Load Step	
	Rich	Lean	Rich	Lean
$\lambda$	0.97	2.0	0.97	2.0
$\text{O}_2$ (%)	1.07	10	1.07	10
$\text{CO}$ (%)	1.6	0.2	1.6	0.2
$\text{H}_2$ (%)	0.8	0	0.8	0
$\text{NO}$ (%)	0.06	0.036	0.12	0.036
$\text{C}_3\text{H}_8$ (%)	0.1	0.06	0.1	0.06
$\text{H}_2\text{O}$ (%)	11	6.6	4.95	6.6
$\text{CO}_2$ (%)	11	6.6	4.95	6.6
$\text{SV}$ ( $\text{hr}^{-1}$ )	27,000	45,000	60,000	45,000

For the cycling experiments, several quantities were calculated. The  $\text{NO}_x$  storage was calculated by integrating the  $\text{NO}_x$  breakthrough during the transition from rich to lean for each cycle. The oxygen storage was calculated by integrating the reductant breakthrough during the transition from rich to lean. The rich phase  $\text{NH}_3$  yield was calculated by measuring the average  $\text{NH}_3$  produced during the rich phase and comparing it to the maximum  $\text{NH}_3$  production assuming all rich phase  $\text{NO}_x$  was converted to  $\text{NH}_3$ . Rich phase CO conversion was calculated by measuring CO slip during the rich phase and comparing it to the CO being flowed during the rich phase. The average  $\text{C}_3\text{H}_8$  conversion was calculated over both the lean and rich phase. To determine projected fuel consumption, in-engine fuel consumption for both fixed load and load step operation was measured directly on a lean-burn gasoline engine under lean and rich conditions [36]. These numbers were then used to calculate the projected fuel consumption based on the amount of time running rich vs. lean using the feedback-controlled cycling shown in Fig. 3. These numbers assume that the downstream SCR catalyst is capable of storing and reducing the requisite  $\text{NO}_x$  during operation.

### **3. Results and Discussion**

#### **3.1 Hydrothermal Aging Progression**

The four-mode hydrothermal aging procedure led to significant sintering of the active metal on Malibu-1 samples. The particle sizes were measured by both STEM and chemisorption at four stages during the aging procedure: a fresh catalyst sample, which has not been aged, as well as samples aged for 25 hours, 50 hours, and 100 hours. The sample that has been aged for 100 hours represents a catalyst at the end of its projected useful life. An example of the contrast

between HAADF and EDX maps are shown in Fig. 4. This comparison illustrates the limitations of using exclusively HAADF to determine particle sizes as the z-contrast is not high enough. However, when EDX maps are implemented, the boundaries between different elements becomes clear, and individual particles can be measured.

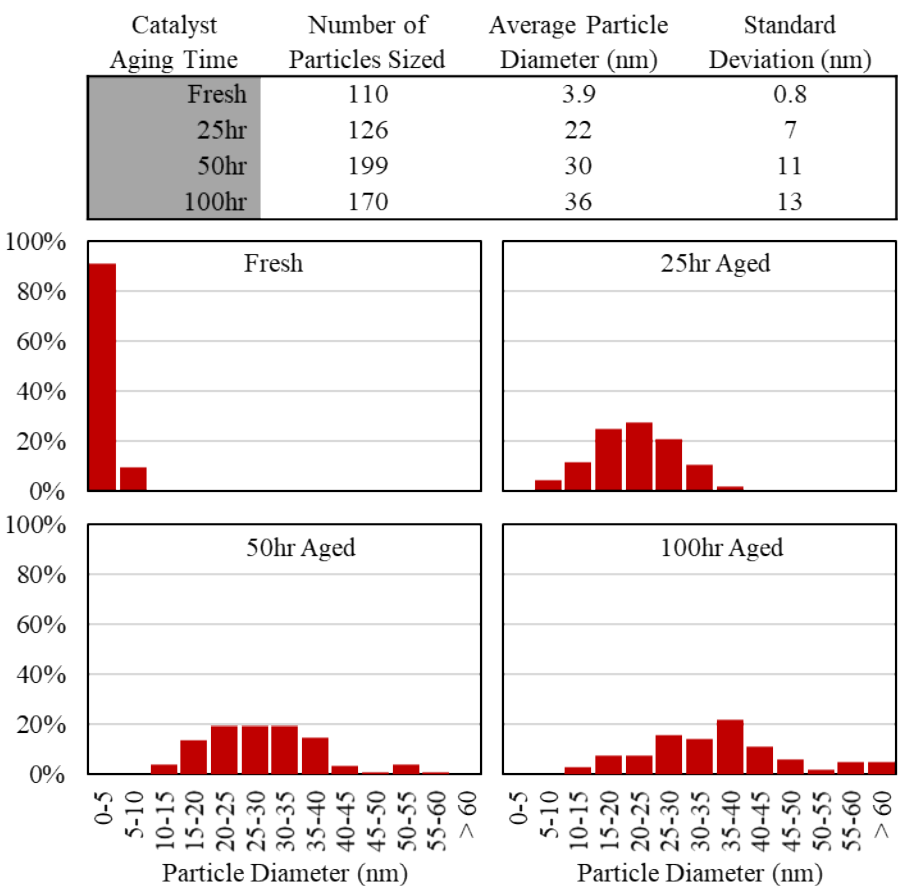


Figure 4: Particle size distribution from STEM for Malibu-1 samples

The particle size distributions for Malibu-1 at each stage of aging, as well as the number of particles analyzed, and their average size are summarized in Table 1. An example of the contrast between HAADF and EDX maps are shown in Fig. 4. This comparison illustrates the limitations of using exclusively HAADF to determine particle sizes as the z-contrast is not high enough. However, when EDX maps are implemented, the boundaries between different elements becomes clear, and individual particles can be measured.

Catalyst Aging Time	Number of Particles Sized	Average Particle Diameter (nm)	Standard Deviation (nm)
Fresh	110	3.9	0.8
25hr	126	22	7
50hr	199	30	11
100hr	170	36	13

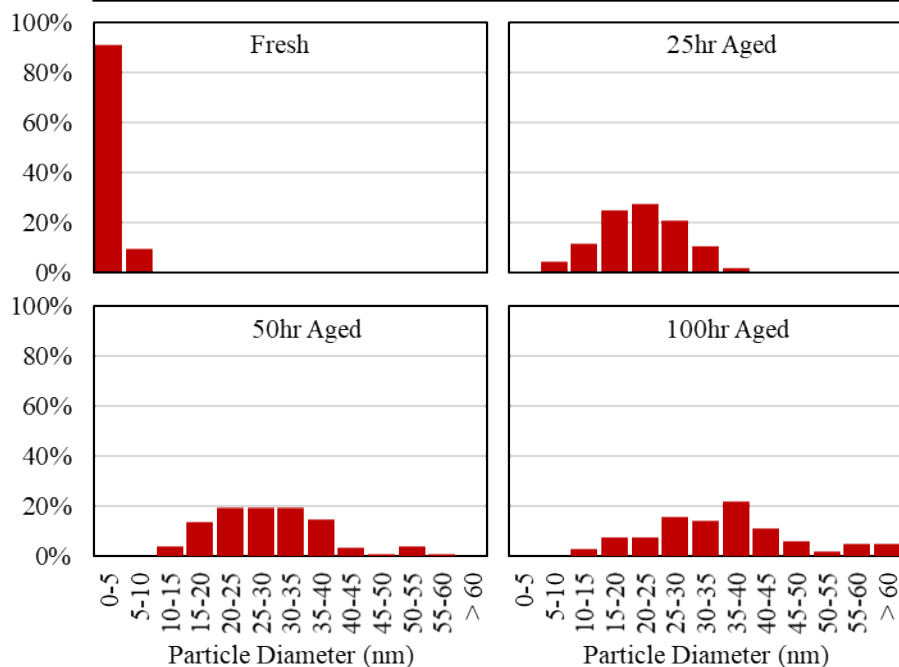


Figure 4. As the catalyst is aged, the average particle size increases from 3.9 nm for the fresh catalyst, to 36 nm for the catalyst aged for 100 hours. In addition to the increase in average particle size, the standard deviation of the particle size also increases from 0.8 nm to 13 nm.

STEM results were supported by hydrogen chemisorption measurements on the catalyst samples. Particle sizes determined for Malibu-1 samples from both STEM and chemisorption tests are summarized in 5. In contrast to STEM measurements, which are 2-D pictures of catalyst particles, chemisorption measures the metal dispersion and calculates the particle size assuming hemispherical particles. Despite the differences in the measurement techniques, the calculated particle sizes show close agreement. While the average diameter of the metal particles is initially less than 5 nm, after 25 hours of aging, the particle size exceeds 20 nm according to both chemisorption and STEM measurements. Continued aging leads to further increased particle sizes

and after the full 100 hours of aging, the average particle size exceeds 30 nm regardless of the method used.

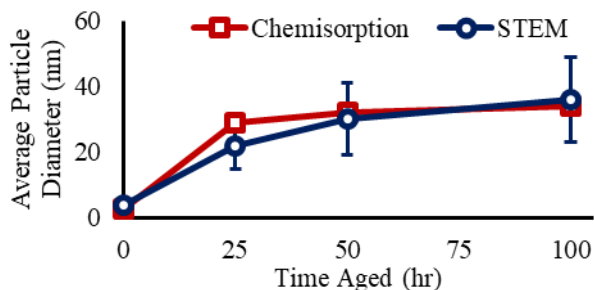


Figure 5: Particle sizing for Malibu-1 catalyst throughout aging

Aging also led to increases in CO light off temperature for both catalysts, which is a concern due to the potential increase in cold-start emissions [32–34].

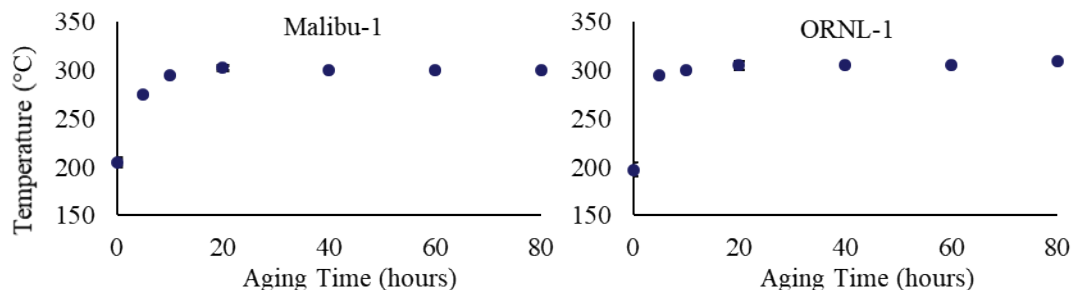


Figure 6 shows the change in light-off temperature for both Malibu-1 and ORNL-1 catalysts as monitored in the aging reactor. The light-off temperature rapidly increases during the first 5-10 hours of aging and remains constant for the remainder of the aging time. This is consistent with previous research, where smaller metal particles have been shown to be more active for low temperature CO oxidation because they can more closely interact with OSC on the catalyst [35,36]. Once the particles begin to sinter, this interaction becomes less effective, which leads to a sharp increase in light off temperature during the initial 10-20 hours of aging. After this initial

increase in light off temperature, the light off temperature stays constant throughout the remaining aging time.

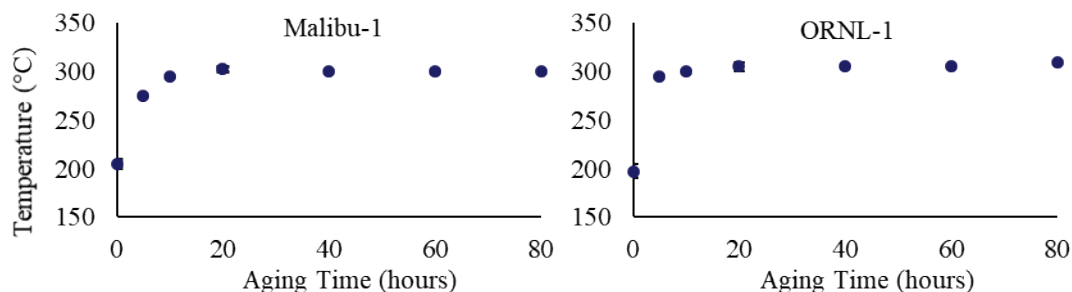


Figure 6: Light off temperature measurements taken during first 80 hours of aging for Malibu-1 and ORNL-1 catalysts

### 3.2 Steady State Activity

The effect of hydrothermal aging on steady state activity was determined through experiments testing fresh catalysts and samples aged for 100 hours. These samples were tested under a range of  $\lambda$  values, as described in section 2.2. The results shown in Figure 7 illustrate the difference between fresh catalysts and aged catalysts. CO and C<sub>3</sub>H<sub>8</sub> slip are increased strongly through hydrothermal aging on the Malibu-1 sample. This deactivation can be attributed to a combination of oxidation activities for the various reductants present in the simulated exhaust, as well as the water gas shift and steam reforming reactions. Small PGM particles improve the activity of these reactions through interactions with the OSC and by increasing the prevalence of interface sites between the PGM and oxide. Interactions between the OSC and the PGM are beneficial for the oxidation reactions, while the interface sites have been shown to be active for the water gas shift reaction [35,37]. When the catalyst is aged and both the PGM and OSC sinter, these interactions are no longer effective, and the prevalence of interface sites is drastically decreased, leading to deactivation in each of these reactions. Decreases in both CO and C<sub>3</sub>H<sub>8</sub> conversion are

also observed for the ORNL-1. However, the ORNL-1 maintains near complete hydrocarbon conversion in the rich phase, even after the full 100 h of aging. This is likely due to the increased activity for the steam reformation reaction originating from the increased ceria loading. Furthermore, while the conversion of CO on the fresh ORNL-1 sample was lower than the conversion on the fresh Malibu-1 sample, the effect of hydrothermal aging on the CO conversion over the ORNL-1 is less than that observed on the Malibu-1. This is particularly evident at  $\lambda$  values above 0.98, where the ORNL-1 maintains the same conversion even after aging. Retention of catalyst activity is likely caused by the presence of substantially higher amounts of OSC on the NSR-TWC, which leads to a higher amount of PGM-OSC interface sites, even after aging. This allows the NSR-TWC to maintain its activity for oxidation, water gas shift, and steam reforming reactions.

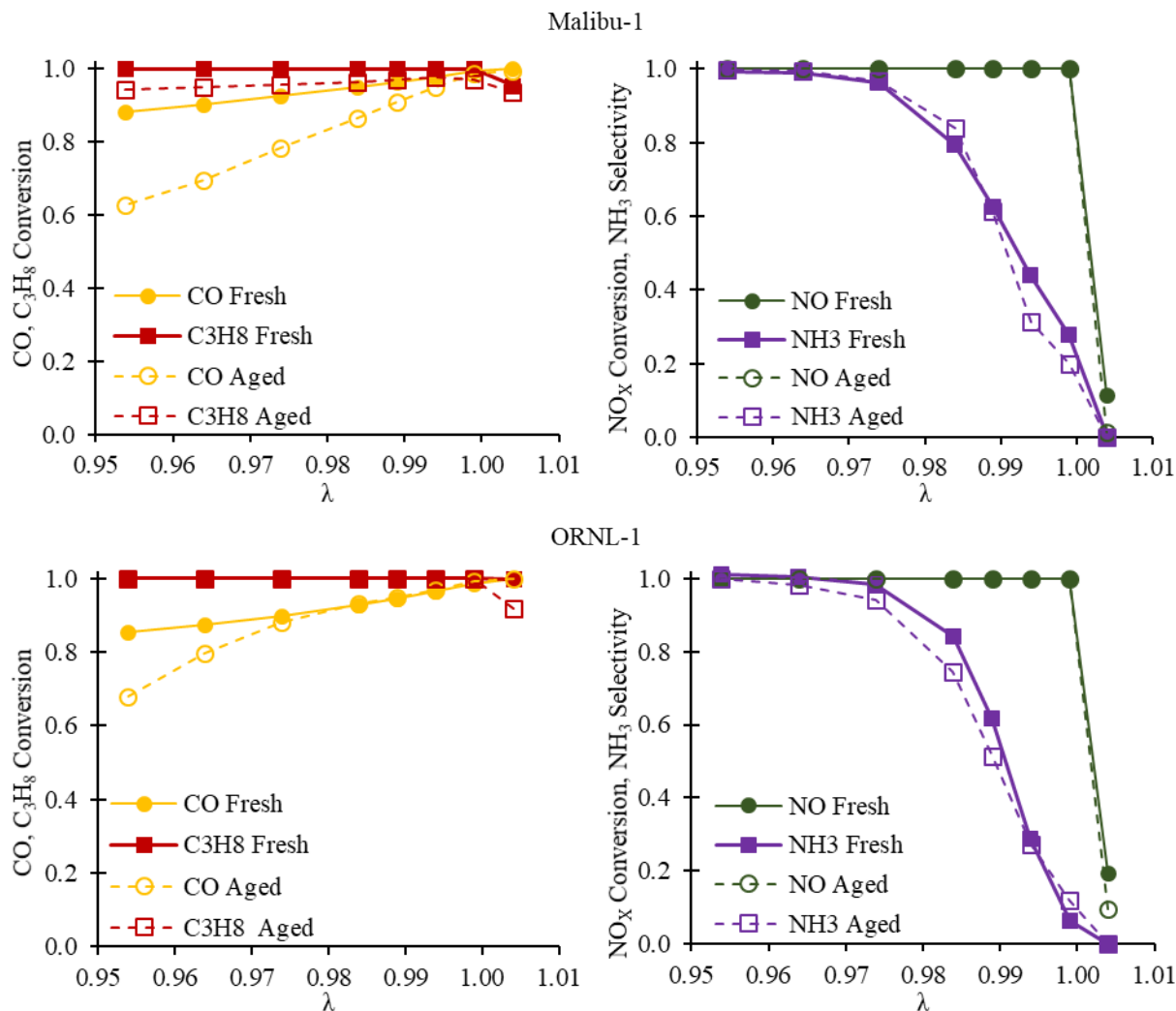


Figure 7: Steady State Activity for Malibu-1 (top) and ORNL-1 (bottom) at 400°C for  $\lambda$  values ranging from 0.95-1.01

In contrast to CO and C<sub>3</sub>H<sub>8</sub> conversion, NO<sub>x</sub> conversion is not strongly affected by hydrothermal aging, maintaining near 100% conversion at both stoichiometric and all rich  $\lambda$  values. Furthermore, the NH<sub>3</sub> selectivity is maintained at nearly 100% when operating at a  $\lambda$  lower than 0.98. While interface sites and OSC interaction will be more important for the removal of CO and C<sub>3</sub>H<sub>8</sub>, the same is not true for NO<sub>x</sub> conversion and NH<sub>3</sub> production, both of which are active

on the bulk PGM surface. Therefore, even though the catalyst undergoes extensive particle sintering, the available PGM surface is still sufficient for NO<sub>x</sub> conversion and NH<sub>3</sub> production.

### 3.3 Cycling Activity

The activity of the catalysts under lean-rich cycling conditions was measured in a bench flow reactor capable of feedback-controlled cycling. The catalysts were cycled between  $\lambda$  values of 0.97 and 2.00, as outlined in Table 4. The measurements taken from the aged catalysts are compared to evaluations conducted on catalysts that were degreened at 700°C for 16 hours. Time series data for the aged sample of Malibu-1 under fixed load and load step conditions at 350°C are shown in Figure 8: Time series data for fixed load and load step conditions on a hydrothermally aged Malibu-1 sample evaluated at 350°C. Under fixed load conditions, where a constant load on the engine is simulated, the time spent in the lean phase and the time spent in the rich phase are relatively similar because the NO<sub>x</sub> flux in the system is constant. However, using load step, where the opportunistic generation of NH<sub>3</sub> during periods of high load is simulated, the rich phase is shorter because increasing the load on the engine results in greatly elevated NO<sub>x</sub> flux, allowing for more NH<sub>3</sub> to be generated. These cycling experiments allow us to simulate catalyst performance under realistic operating conditions. They also allow us to capture the effects of hydrothermal aging on oxygen and NO<sub>x</sub> storage capacity by studying the lean-rich transitions. This is particularly important for ORNL-1, which includes significant levels of OSC and NSC, both of which showed significant deactivation during aging.

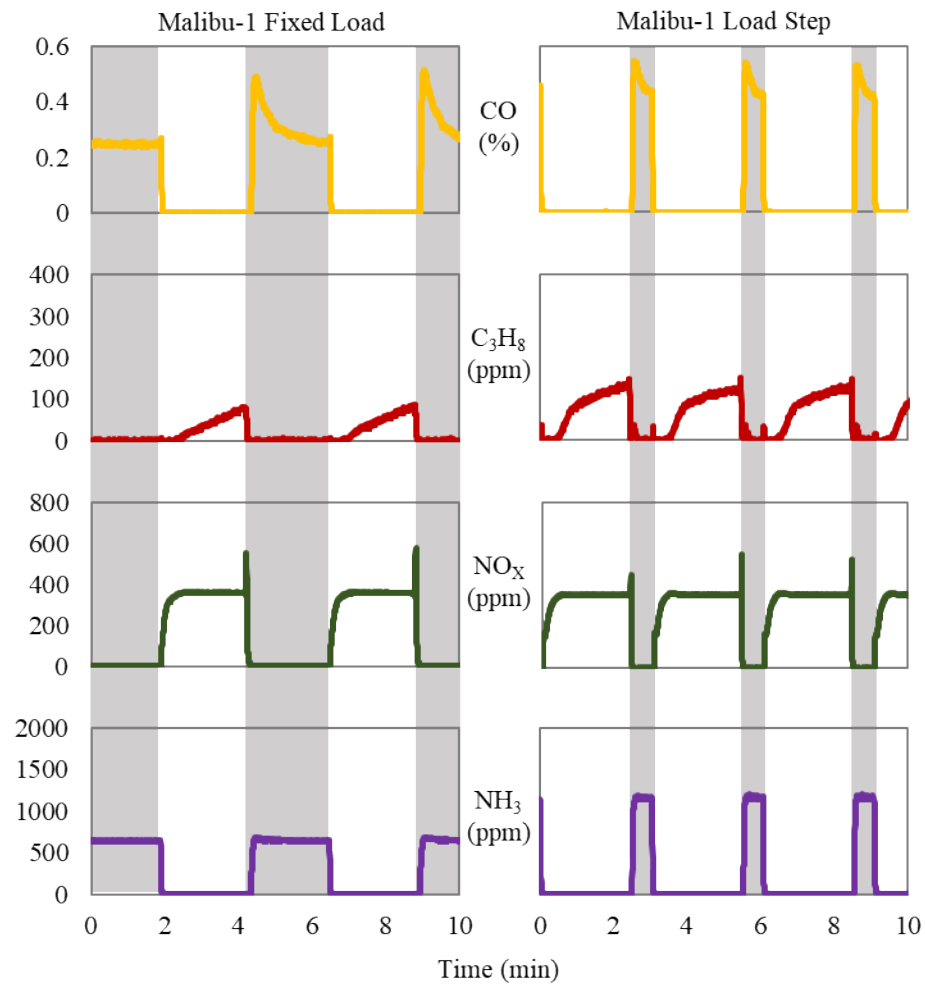


Figure 8: Time series data for fixed load and load step conditions on a hydrothermally aged Malibu-1 sample evaluated at 350°C.

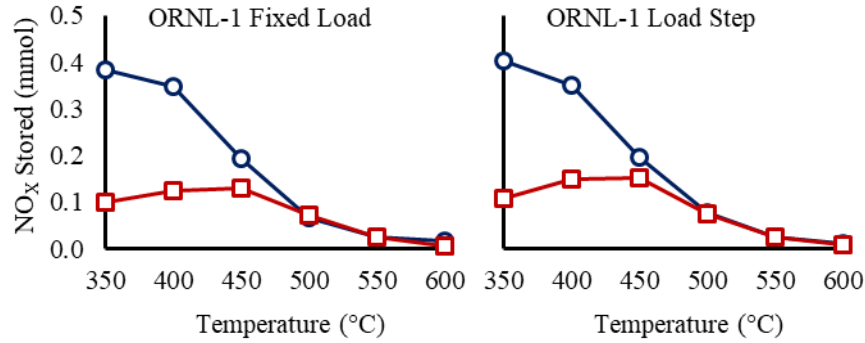


Figure 9: Average NO<sub>x</sub> stored per cycle on ORNL-1 under both fixed load (left) and load step (right) conditions for degreened (circles) and aged (square) samples

Figure 9 shows the strong deactivation of NSC from hydrothermal aging on the ORNL-1 catalyst. At 350°C, the amount of NO<sub>x</sub> stored on the aged catalyst is roughly 25% of that on the degreened sample. This is significant because it inhibits the primary advantage of using a NSR-type catalyst for passive SCR: using NSC to prolong the lean phase. The deactivation mechanisms of the primary NSC Ba have been studied by previous researchers [29]. It has been shown that the primary mechanism for the loss of NSC is the formation of barium aluminate and cerate on the surface. This formation occurs above 800°C for the cerate and above 850°C for the aluminate. Therefore, the sample degreened at 700°C does not lose NSC through this mechanism, but the sample aged at 920°C loses a significant amount of NSC by forming these highly stable species. Because ORNL-1 loses a majority of its NO<sub>x</sub> storage, the amount of time the system can operate lean is decreased, which will cause a net increase in projected fuel consumption; therefore, for this application and this catalyst it would be preferred to not exceed 850°C.

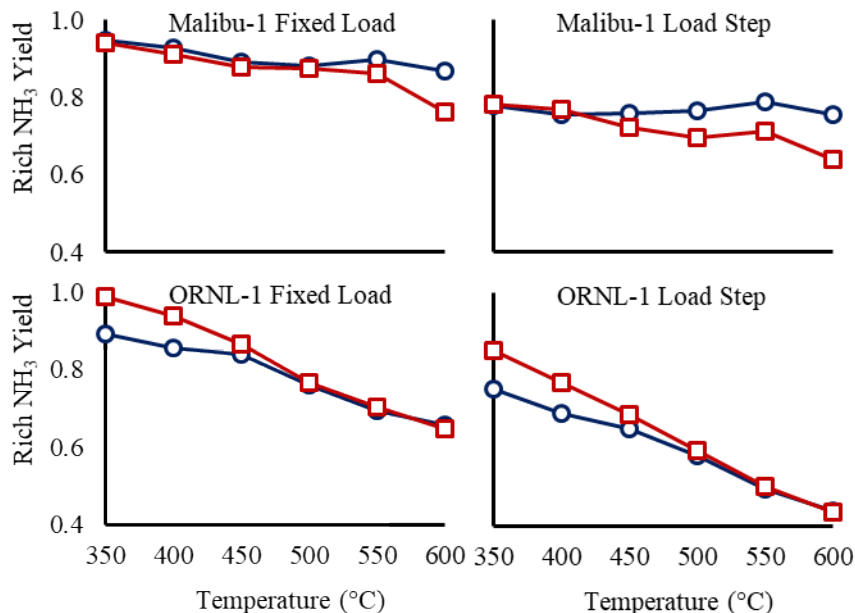


Figure 10: Rich phase NH<sub>3</sub> yield for Malibu-1 (top) and ORNL-1 (bottom) for both fixed load (left) and load step (right) conditions comparing degreened (circles) and aged (squares) samples

Figure 10 shows the changes in OSC from hydrothermal aging for both Malibu-1 and ORNL-1. On Malibu-1, the low temperature activity for NH<sub>3</sub> production remains unchanged, which is consistent with results from steady state experiments. However, at higher temperatures, the aged catalyst shows decreased activity. In contrast to Malibu-1, the NH<sub>3</sub> yield on the aged ORNL-1 sample is increased at temperatures below 450°C, and similar to the degreened activity above 450°C. The primary cause for this is the deactivation of the OSC on ORNL-1. OSC deactivation has been shown to be a result of increase in cerium oxide particle size [28]. During the transition from lean to rich, the catalyst must be reduced before the production of NH<sub>3</sub> can begin. Because the hydrothermal aging procedure leads to significant loss of OSC on ORNL-1, it allows for production of NH<sub>3</sub> in the rich phase to begin more quickly, as shown in Figure 11.

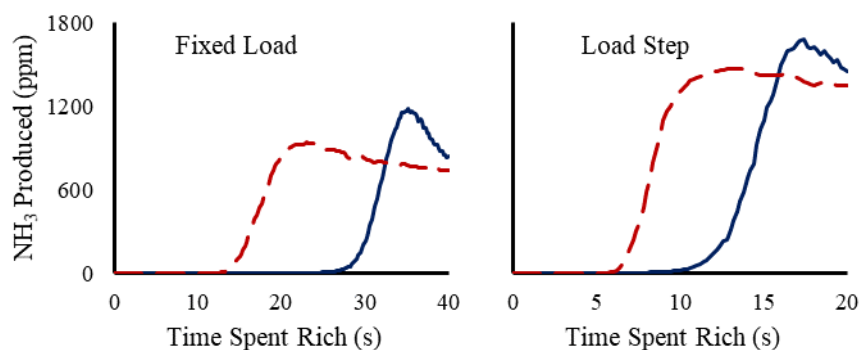


Figure 11: NH<sub>3</sub> breakthrough during rich operation on ORNL-1 at 350°C comparing degreened (solid) and aged (dashed) samples

Figure 12 shows the effects of hydrothermal aging on CO conversion. The primary effect on both catalysts is a decrease in CO conversion at low temperatures, while at higher temperatures, the degreened and aged activities are closer. This is consistent with steady state results and light off curves, which showed a strong decrease in CO oxidation activity at low temperature. As discussed previously, these low temperature changes are likely attributed to the loss of active surface area as well as PGM-OSC interface sites. On ORNL-1, the low temperature CO conversion was not as strongly deactivated as on Malibu-1, which is consistent with results from the steady state experiments.

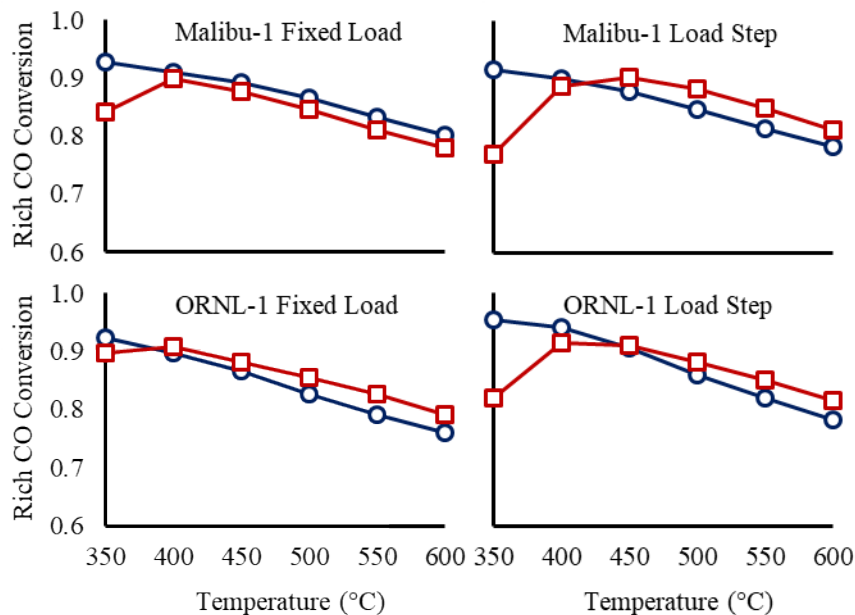


Figure 12: Rich phase CO conversion for Malibu-1 (top) and ORNL-1 (bottom) for both fixed load (left) and load step (right) conditions comparing degreened (circles) and aged (squares) samples

The effect of hydrothermal aging on overall  $C_3H_8$  conversion is shown in Figure 13. Malibu-1 shows slight  $C_3H_8$  breakthrough at 350°C. Under both fixed load and load step conditions, there is no significant change in the  $C_3H_8$  conversion and both the aged and the degreened Malibu-1 samples show similar concentrations of  $C_3H_8$  in the outlet. However, on ORNL-1, the  $C_3H_8$  conversion is significantly lower compared to Malibu-1. Furthermore, the aged sample shows better average conversion than the degreened sample. This is primarily due to the deactivation of the NSC on ORNL-1 during hydrothermal aging. Because the degreened sample retains a large amount of NSC, as shown in Figure 9, the lean phase lasts longer than it does when the aged sample is used. This leads to a longer time that the catalyst is under oxidizing conditions, leading to higher  $C_3H_8$  slip.

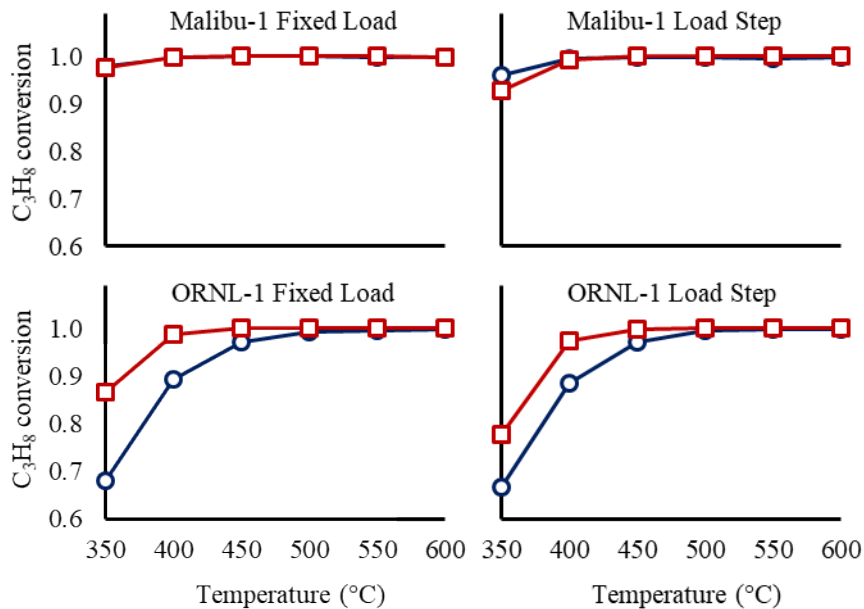


Figure 13: Average C<sub>3</sub>H<sub>8</sub> conversion for Malibu-1 (top) and ORNL-1 (bottom) for both fixed load (left) and load step (right) conditions comparing degreened (circles) and aged (red) samples

The projected fuel consumption relative to stoichiometric operation is shown in Figure 14. To determine projected fuel consumption, in-engine fuel consumption for both fixed load and load step operation was measured directly on a lean-burn gasoline engine under lean and rich conditions [38]. These numbers were then used to calculate the projected fuel consumption based on the amount of time running rich vs. lean using the feedback-controlled cycling shown in Figure 3. While CO and C<sub>3</sub>H<sub>8</sub> emissions are a concern, they do not affect the projected fuel consumption because they do not influence the feedback-controlled cycling. The only factors that will have an effect are NH<sub>3</sub> production, NO<sub>x</sub> conversion, and NO<sub>x</sub> storage. On Malibu-1, the projected fuel consumption benefits at high temperatures are slightly decreased due to the decrease in the NH<sub>3</sub> production on the aged catalyst. This increases the length of time the system must operate under fuel rich conditions, during which the fuel consumption is increased. However, the low temperature projected fuel consumption remains unchanged. On ORNL-1, the projected fuel

consumption benefit is decreased at lower temperatures due to the loss of NSC. This causes shorter lean phases at low temperatures and, by extension, higher projected fuel consumption. The loss of OSC proved beneficial on ORNL-1 because it allowed for a more rapid breakthrough of  $\text{NH}_3$  during the rich phase. Despite the effects of aging, both catalysts maintained sufficient activity to operate a passive SCR system, with projected fuel consumption ranging from 91-98% of stoichiometric fuel consumption in the temperature range observed.

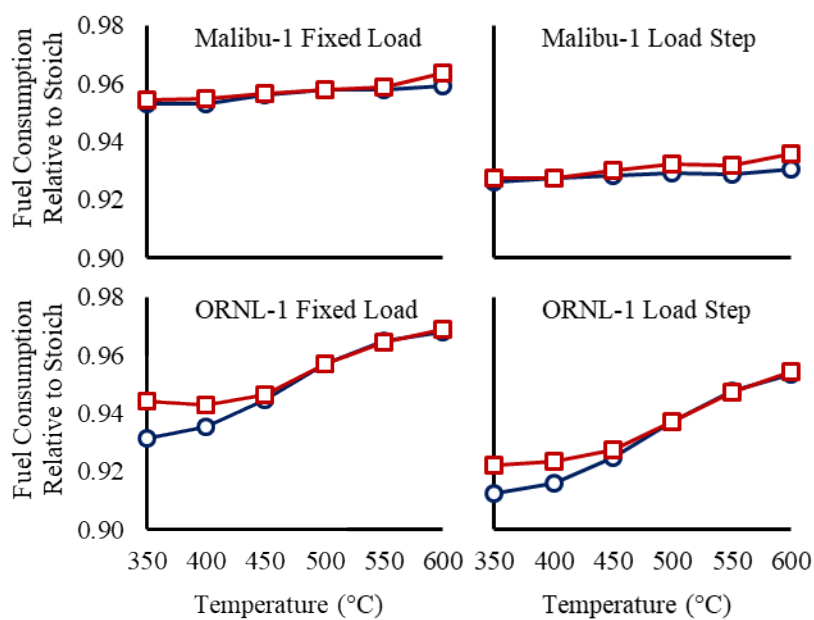


Figure 14: Projected fuel consumption for Malibu-1 (top) and ORNL-1 (bottom) for both fixed load (left) and load step (right) conditions comparing degreened (circles) and aged (squares) samples

#### 4. Conclusions

Hydrothermal aging using a four-stage aging protocol lead to significant deactivation in two fully formulated commercial automotive catalysts. The primary means of deactivation is the sintering of the active metal, with the average diameter of palladium particles on Malibu-1

increasing from  $< 5$  nm to  $> 30$  nm over the course of 100 hours of aging. The CO light off temperature also increased due to aging, particularly during the first 25 hours. After aging, the steady state activity of the two catalysts was measured using simulated exhaust gas mixtures approximating a wide range of  $\lambda$  values at 400°C. In these experiments, Malibu-1 showed significantly decreased activity for CO and C<sub>3</sub>H<sub>8</sub> conversion. However, ORNL-1 was not as strongly affected, and maintained higher steady state activity for the conversion of CO and C<sub>3</sub>H<sub>8</sub>. This difference could be attributed to the high loading of OSC on ORNL-1, which allows it to maintain higher activity for water gas shift and steam reforming reactions, as well as providing interface sites between the PGM and the oxide support, which have been shown to be more active for low temperature oxidation. Despite the extensive hydrothermal aging, catalyst deactivation did not extend to the reduction of NO<sub>x</sub> to NH<sub>3</sub>. Both catalysts maintained close to 100% steady state selectivity to NH<sub>3</sub> for all  $\lambda$  values lower than 0.98.

Transient studies allowed for further probes into the effects of aging. Many of the results from steady state tests were corroborated, including the effects on NH<sub>3</sub>, CO, and C<sub>3</sub>H<sub>8</sub>. However, under cycling conditions, the effects of OSC and NSC were far more pronounced. There was significant levels of Ce and Ba degradation on ORNL-1 through aging, significantly affecting the cycling activity compared to a degreened sample. The loss of NSC led to shorter lean phases on the aged catalyst, causing higher projected fuel consumption. Deactivation of the OSC proved beneficial for the system, as it caused the catalyst to be reduced more quickly in the rich phase, allowing for more rapid breakthrough of NH<sub>3</sub>, leading to a shorter rich phase and reducing the overall fuel penalty accrued while running rich. Overall, while the four-mode hydrothermal aging procedure led to significant particle sintering, as well as loss of OSC and NSC, the aged catalysts

still proved effective in producing the necessary NH<sub>3</sub> for the operation of a passive SCR system with projected fuel consumption ranging from 91 to 98% compared to stoichiometric operation.

### **Acknowledgements:**

*Funding was provided by Department of Energy Vehicle Technologies Office and the South Carolina Smartstate Center for Strategic Approaches to the Generation of Electricity (SAGE) at the University of South Carolina. Additionally, a portion of this research was performed using instrumentation (FEI Talos F200X S/TEM) provided by the Department of Energy, Office of Nuclear Energy, Fuel Cycle R&D Program and the Nuclear Science User Facilities.*

### **References**

- [1] S.C. Davis, S.E. Williams, R.G. Boundy, Transportation Energy Data Book Edition 36, 2017. [http://cta.ornl.gov/data/tedb36/Edition\\_36\\_Full\\_Doc.pdf](http://cta.ornl.gov/data/tedb36/Edition_36_Full_Doc.pdf).
- [2] The U.S. Environmental Protection Agency (EPA), Direct Final Rulemaking for EPA Tier 3 Emission and Fuel Standards, 80 (2015).
- [3] J.E. Parks, V. Prikhodko, W. Partridge, J.-S. Choi, K. Norman, S. Huff, P. Chambon, Lean Gasoline Engine Reductant Chemistry During Lean NO<sub>x</sub> Trap Regeneration, SAE Int. J. Fuels Lubr. 3 (2010) 2010-01–2267. doi:10.4271/2010-01-2267.
- [4] S. Roy, M.S. Hegde, G. Madras, Catalysis for NO<sub>x</sub> abatement, Appl. Energy. 86 (2009) 2283–2297. doi:10.1016/j.apenergy.2009.03.022.
- [5] S. Matsumoto, DeNO<sub>x</sub> catalyst for automotive lean-burn engine, Catal. Today. 29 (1996) 43–45. doi:10.1016/0920-5861(95)00259-6.
- [6] E. Fridell, M. Skoglundh, B. Westerberg, S. Johansson, G. Smedler, NO<sub>x</sub> storage in

- barium-containing catalysts, *J. Catal.* 183 (1999) 196–209. doi:10.1006/jcat.1999.2415.
- [7] J.S. Choi, W.P. Partridge, J.A. Pihl, M.Y. Kim, P. Kočí, C.S. Daw, Spatiotemporal distribution of NO<sub>x</sub> storage and impact on NH<sub>3</sub> and N<sub>2</sub>O selectivities during lean/rich cycling of a Ba-based lean NO<sub>x</sub> trap catalyst, *Catal. Today*. 184 (2012) 20–26. doi:10.1016/j.cattod.2011.11.007.
- [8] W.S. Epling, L.E. Campbell, A. Yezerets, N.W. Currier, J.E. Parks, Overview of the fundamental reactions and degradation mechanisms of NO<sub>x</sub> storage/reduction catalysts, *Catal. Rev. - Sci. Eng.* 46 (2004) 163–245. doi:10.1081/CR-200031932.
- [9] T. Johnson, Diesel engine emissions and their control: An overview, *Platin. Met. Rev.* 52 (2008) 23–37. doi:10.1595/147106708X248750.
- [10] A. Russell, W.S. Epling, Diesel oxidation catalysts, *Catal. Rev. - Sci. Eng.* 53 (2011) 337–423. doi:10.1080/01614940.2011.596429.
- [11] M. Shelef, R.W. McCabe, Twenty-five years after introduction of automotive catalysts: what next?, *Catal. Today*. 62 (2000) 35–50. doi:10.1016/S0920-5861(00)00407-7.
- [12] R.M. Heck, R.J. Farrauto, Automobile exhaust catalysts, *Appl. Catal. A Gen.* 221 (2001) 443–457. doi:10.1016/S0926-860X(01)00818-3.
- [13] T. V. Johnson, Review of Vehicular Emissions Trends, *SAE Int. J. Engines.* 8 (2015) 2015-01–0993. doi:10.4271/2015-01-0993.
- [14] A. Sultana, T. Nanba, M. Sasaki, M. Haneda, K. Suzuki, H. Hamada, Selective catalytic reduction of NO<sub>x</sub> with NH<sub>3</sub> over different copper exchanged zeolites in the presence of decane, *Catal. Today*. 164 (2011) 495–499. doi:10.1016/j.cattod.2010.11.036.
- [15] T.V.W. Janssens, H. Falsig, L.F. Lundegaard, P.N.R. Vennestrøm, S.B. Rasmussen, P.G. Moses, F. Giordanino, E. Borfecchia, K.A. Lomachenko, C. Lamberti, S. Bordiga, A.

- Godiksen, S. Mossin, P. Beato, A consistent reaction scheme for the selective catalytic reduction of nitrogen oxides with ammonia, *ACS Catal.* 5 (2015) 2832–2845.  
doi:10.1021/cs501673g.
- [16] T.L. McKinley, A.G. Alleyne, Adaptive Model Predictive Control of an SCR Catalytic Converter System for Automotive Applications, *Control Syst. Technol. IEEE Trans.* 20 (2012) 1533–1547. doi:10.1109/TCST.2011.2169494.
- [17] Q. Song, G. Zhu, Model-based Closed-loop Control of Urea SCR Exhaust Aftertreatment System for Diesel Engine, *SAE Tech. Pap.* (2002). doi:10.4271/2002-01-0287.
- [18] C.H. Kim, K. Perry, M. Viola, W. Li, K. Narayanaswamy, Three-Way Catalyst Design for Urealess Passive Ammonia SCR: Lean-Burn SIDI Aftertreatment System, in: *SAE Tech. Pap.* 2011-01-0306, 2011. doi:10.4271/2011-01-0306.
- [19] K. Rahkamaa-Tolonen, Investigation of NO Reduction by H<sub>2</sub> on Pd Monolith with Transient and Isotopic Exchange Techniques II. H<sub>2</sub>/D<sub>2</sub> Exchange in the Reduction of NO, *J. Catal.* 210 (2002) 30–38. doi:10.1006/jcat.2002.3669.
- [20] S.H. Oh, T. Triplett, Reaction pathways and mechanism for ammonia formation and removal over palladium-based three-way catalysts: Multiple roles of CO, *Catal. Today.* 231 (2014) 22–32. doi:10.1016/j.cattod.2013.11.048.
- [21] E.C. Adams, M. Skoglundh, M. Folic, E.C. Bendixen, P. Gabrielsson, P.A. Carlsson, Ammonia formation over supported platinum and palladium catalysts, *Appl. Catal. B Environ.* 165 (2015) 10–19. doi:10.1016/j.apcatb.2014.09.064.
- [22] V.Y. Prikhodko, J.E. Parks, J.A. Pihl, T.J. Toops, Ammonia Generation and Utilization in a Passive SCR (TWC+SCR) System on Lean Gasoline Engine, *SAE Int. J. Engines.* 9 (2016) 2016-01–0934. doi:10.4271/2016-01-0934.

- [23] Q. Xu, K.C. Kharas, B.J. Croley, A.K. Datye, The Sintering of Supported Pd Automotive Catalysts, *ChemCatChem*. 3 (2011) 1004–1014. doi:10.1002/cctc.201000392.
- [24] H. Arai, M. Machida, Thermal stabilization of catalyst supports and their application to high-temperature catalytic combustion, *Appl. Catal. A Gen.* 138 (1996) 161–176. doi:10.1016/0926-860X(95)00294-4.
- [25] A. Iglesias-Juez, A. Martínez-Arias, M. Fernández-García, Metal-promoter interface in Pd/(Ce,Zr)Ox/Al<sub>2</sub>O<sub>3</sub> catalysts: Effect of thermal aging, *J. Catal.* 221 (2004) 148–161. doi:10.1016/j.jcat.2003.07.010.
- [26] S. Suhonen, M. Valden, M. Pessa, A. Savimäki, M. Härkönen, M. Hietikko, J. Pursiainen, R. Laitinen, Characterization of alumina supported Pd catalysts modified by rare earth oxides using X-ray photoelectron spectroscopy and X-ray diffraction: Enhanced thermal stability of PdO in Nd/Pd catalysts, *Appl. Catal. A Gen.* 207 (2001) 113–120. doi:10.1016/S0926-860X(00)00621-9.
- [27] A. Martínez-Arias, M. Fernández-García, A. Iglesias-Juez, A.B. Hungría, J.A. Anderson, J.C. Conesa, J. Soria, Influence of thermal sintering on the activity for CO-O<sub>2</sub> and CO-O<sub>2</sub>-NO stoichiometric reactions over Pd/(Ce, Zr)Ox/Al<sub>2</sub>O<sub>3</sub> catalysts, *Appl. Catal. B Environ.* 38 (2002) 151–158. doi:10.1016/S0926-3373(02)00033-4.
- [28] A. Fathali, L. Olsson, F. Ekström, M. Laurell, B. Andersson, Hydrothermal aging-induced changes in washcoats of commercial three-way catalysts, *Top. Catal.* 56 (2013) 323–328. doi:10.1007/s11244-013-9974-8.
- [29] M. Casapu, J.D. Grunwaldt, M. Maciejewski, M. Wittrock, U. Göbel, A. Baiker, Formation and stability of barium aluminate and cerate in NO<sub>x</sub> storage-reduction catalysts, *Appl. Catal. B Environ.* 63 (2006) 232–242. doi:10.1016/j.apcatb.2005.10.003.

- [30] J. Parks, T.J. Toops, J.A. Pihl, Emissions Control for Lean Gasoline Engines, (2015).  
[https://www.energy.gov/sites/prod/files/2015/06/f23/ace033\\_parks\\_2015\\_o.pdf](https://www.energy.gov/sites/prod/files/2015/06/f23/ace033_parks_2015_o.pdf) (accessed March 14, 2018).
- [31] C.M. Parish, MT3FT-15OR0204122: Report on the acquisition and installation of FEI Talos F200X S/TEM., ORNL/LTR-2015/461. Oak Ridge Natl. Lab. (ORNL), Oak Ridge, TN (United States). (2015) 1–7.
- [32] M. Clairotte, T.W. Adam, A.A. Zardini, U. Manfredi, G. Martini, A. Krasenbrink, A. Vicet, E. Tournié, C. Astorga, Effects of low temperature on the cold start gaseous emissions from light duty vehicles fuelled by ethanol-blended gasoline, *Appl. Energy*. 102 (2013) 44–54. doi:10.1016/j.apenergy.2012.08.010.
- [33] M.Y. Kim, E.A. Kyriakidou, J.S. Choi, T.J. Toops, A.J. Binder, C. Thomas, J.E. Parks, V. Schwartz, J. Chen, D.K. Hensley, Enhancing low-temperature activity and durability of Pd-based diesel oxidation catalysts using ZrO<sub>2</sub> supports, *Appl. Catal. B Environ.* 187 (2016) 181–194. doi:10.1016/j.apcatb.2016.01.023.
- [34] C. Wang, A.J. Binder, T.J. Toops, J. Lauterbach, E. Sasmaz, Evaluation of Mn and Sn-Modified Pd-Ce-Based Catalysts for Low-Temperature Diesel Exhaust Oxidation, *Emiss. Control Sci. Technol.* 3 (2017) 37–46. doi:10.1007/s40825-016-0056-9.
- [35] A.I. Boronin, E.M. Slavinskaya, I.G. Danilova, R. V. Gulyaev, Y.I. Amosov, P.A. Kuznetsov, I.A. Polukhina, S. V. Koscheev, V.I. Zaikovskii, A.S. Noskov, Investigation of palladium interaction with cerium oxide and its state in catalysts for low-temperature CO oxidation, *Catal. Today*. 144 (2009) 201–211. doi:10.1016/j.cattod.2009.01.035.
- [36] I. Heo, J.W. Choung, P.S. Kim, I.S. Nam, Y. Il Song, C.B. In, G.K. Yeo, The alteration of the performance of field-aged Pd-based TWCs towards CO and C<sub>3</sub>H<sub>6</sub> oxidation, *Appl.*

- Catal. B Environ. 92 (2009) 114–125. doi:10.1016/j.apcatb.2009.07.016.
- [37] T. Bunluesin, R.J. Gorte, G.W. Graham, Studies of the water-gas-shift reaction on ceria-supported Pt, Pd, and Rh: Implications for oxygen-storage properties, Appl. Catal. B Environ. 15 (1998) 107–114. doi:10.1016/S0926-3373(97)00040-4.
- [38] V.Y. Prikhodko, J.E. Parks, J.A. Pihl, T.J. Toops, Passive SCR for lean gasoline NOX control: Engine-based strategies to minimize fuel penalty associated with catalytic NH<sub>3</sub> generation, Catal. Today. 267 (2016) 202–209. doi:10.1016/j.cattod.2016.01.026.